Maximum-Likelihood Parameter Estimation for the Thin-Shell Quasi-Newtonian Model for a Laboratory Blown Film Extruder

J. C. Pirkle, Jr., M. Fujiwara, and R. D. Braatz*

University of Illinois at Urbana−Champaign, 600 South Mathews Avenue, Urbana, Illinois 61801

While most plastic films are manufactured by blown film extrusion, their first-principles modeling has remained substantially more challenging than for most other chemical engineering unit operations due to its combination of heat transfer, crystallization, and non-Newtonian fluid mechanics. This paper applies maximum-likelihood parameter estimation to characterize the convective heat transfer characteristics from measured spatial radii and temperature profiles for a laboratory-scale blown film process extruding a linear low density polyethylene (LLDPE) polymer. The Pearson and Petrie thin-film extrusion model incorporates (i) a quasi-Newtonian constitutive relation for the effect of temperature and crystallization on the viscosity of the polymer and (ii) a spatial variation of the heat transfer coefficient that is qualitatively consistent with turbulent flow simulations reported in the literature. A single heat transfer expression fit the experimental conditions for a cooling air flow rate of 1.5 m/s, whereas the variation of two parameters was able to fit all but one experimental condition for a cooling air flow rate of 1.0 m/s. The experimental condition that was poorly fit by the model had the highest takeup ratio, which was the operating condition closest to film instability and likely the condition most sensitive to the heat transfer relation. The experimental conditions corresponding to observed stable operations were investigated by linearized stability analysis.

Introduction

Blown film extrusion has been a standard method of manufacturing plastic film for decades,[1,2] including for the packaging of medical products, foodstuffs, agricultural products, and clothing. Molten polymer is extruded through an annular die while air is fed through an inner concentric bubble-tube (see Figure 1). This internal air inflates the cylindrical film, increasing the radius of the polymer bubble by stretching, and decreasing the film thickness. Simultaneously, the nip rolls above the die flatten the film and maintain tension in the axial (upward from the die) direction. External air supplied from a concentric outer ring cools the film. The resulting temperature reduction increases the viscosity of the rising film and eventually induces crystallization as the temperature drops below the melting point of the polymer. The crystallization, in turn, causes an additional increase in viscosity, and the polymer solidifies.

There is a sizable literature that fits mathematical models of blown film extrusion to experimental data for polyethylene (high density, low density, and linear low density), polypropylene, and polystyrene. Most of these efforts involve matching steady-state conditions to experimental data from small-scale extruders. The model computations are mostly carried out by direct solution of the steady-state equations. In some cases, dynamic models have been integrated to steady-state conditions to fit data.[3,4] The models have mostly consisted of the thin-shell model of Pearson and Petrie[5−7] and the quasi-cylindrical (QC) model of Liu and co-workers[8−10] that was further investigated by McHugh and collaborators[11−13] and by Pirkle and Braatz.[4]

The thin-shell model includes the second derivative of the bubble radius in the momentum equation in the hoop, or circumferential, direction. An extra boundary condition is required, which is usually met in steady-state solutions by setting the slope of the bubble radius to zero at an assumed freeze line. The QC model requires no additional boundary condition. All boundary conditions are set at the die position, and the governing differential equations are integrated from the die to the freeze line or beyond. This enables steady-state solutions to be obtained as a rapidly solved initial value problem consisting of ordinary differential equations (ODEs). The ease of computation encouraged use of the QC model in fitting small-scale experiments.[8,12,13] A drawback of the QC model is that it can produce inaccurate results when applied to a wider range of operations. For instance, the QC model predicts blowup ratio versus thickness-reduction curves that are very different from those of the thin-shell model.[4] This suggests that the thin-shell model should be preferred in spite of its computational difficulties.

Several types of constitutive relations have been used to fit model predictions to laboratory data. These include quasi-Newtonian models,[8,9,14,15] microstructural models,[11,16] plastic−elastic transition models,[17] the PPT model,[18−20] and a modified Kelvin model.[21,22] Integral constitutive equations have also been

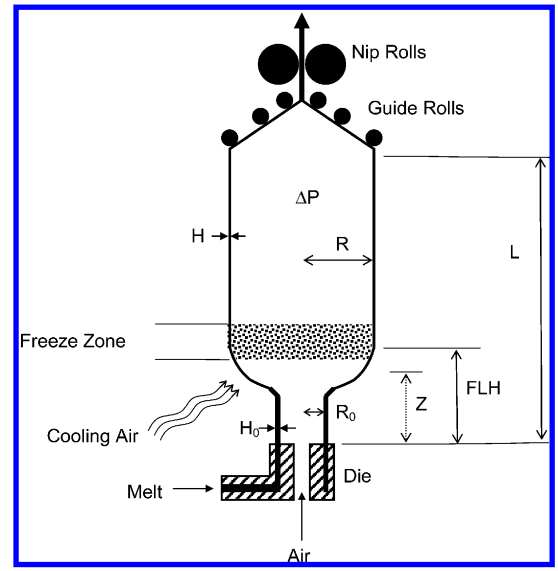

Figure 1. Schematic of blown film extrusion.

* To whom correspondence should be addressed. Telephone: 217-333-5073. Fax: 217-333-5052. E-mail: braatz@illinois.edu.

10.1021/ie100188g
Published on Web 04/08/2010

Table 1. Symbols for Dimensional Variables and Constants

C_{pf}	specific heat of polymer, kJ/kg·K
H_0	film thickness as it exits the die at $Z = 0$, cm
H	film thickness at axial position Z, cm
H_L	film thickness at top boundary of freeze zone, cm
k_{crys}	crystallization rate coefficient, 1/s
L	axial position corresponding to top boundary of freeze zone, cm
M_{air}	bubble air mass, kg·mol
N_Z	number of grid points in discretization of axial coordinate
P_{atm}	atmospheric pressure, Pa
R	radius of film bubble tube at axial position Z, cm
R_G	universal gas constant, kJ/kg·mol·K
R_L	final radius of film bubble tube at top boundary of freeze zone, cm
R_0	radius of film bubble tube as it exits the die at $Z = 0$, cm
t	time, s
T	temperature of film bubble tube at position Z, K
T_{air}	temperature of cooling air, K
T_{max}	temperature at the maximum crystallization rate, K
T_w	temperature of walls of surrounding extruder, K
T_0	temperature of film bubble tube as it exits die at $Z = 0$, K
U_h	heat transfer coefficient between film and external air, W/m^2·K
V	velocity of film at axial position Z, cm/s
V_L	velocity of film at top boundary of freeze zone, cm/s
V_0	velocity of film as it exits the die at $Z = 0$, cm/s
Z	axial position measured upward from position of die, cm
α_1	adjustment coefficient for viscosity factor, Pa·s
α_2	adjustment coefficient for crystallization term in viscosity factor
β_1	adjustment coefficient for temperature dependence of viscosity factor, K
β_2	exponent for crystallization dependence of viscosity factor
X	local fraction of crystallinity, kg of crystalline phase/kg of polymer
X_f	maximum fraction of crystalline phase possible, kg/kg
ΔH_{crys}	heat of crystallization, kJ/kmol
ΔP	inflation pressure, relative to ambient pressure, Pa
ΔT_{max}	width of Gaussian curve at one-half-maximum crystallization rate
ε	radiation emissivity of polymer
ρ	polymer density, kg/m^3
μ	viscosity of polymer, Pa·s
μ_0	viscosity of polymer as it exits die, Pa·s
σ_B	Stefan−Boltzmann radiation constant = 5.670×10^{-8} J/K^4·m^2·s

investigated.[23] Some investigators have included crystallization kinetics and the effect of crystallization on rheological properties.[3,4,8,9,11,12,20] In these studies, the stiffening effect caused by crystallization provides a strong resistance to further expansion of the bubble-tube. The axial position at which expansion ceases is called the *frost line*, which is often significantly below the nip rolls (Figure 1).

Few modeling studies for blown film extrusion have included turbulent fluid mechanics calculations for the air inside and outside of the tubular film (an exception is ref 24) because (i) the high computational cost limits the usefulness of such models for controller design and stability analysis and (ii) the governing equations for the polymer only require the heat transfer characteristics rather than the entire 2D or 3D velocity and stress fields. This paper demonstrates the maximum-likelihood estimation, from experimental data, of parameters characterizing the heat transfer characteristics in a thin-shell model with a quasi-Newtonian constitutive relation for the polymer crystallization. The experimental data are collected from a laboratory-scale blown film extruder. A description of the model, numerical methods, and experimental system is followed by results, discussion, and conclusions.

Dynamic Thin-Shell Model

This dynamic model of film motion neglects inertial terms, surface tension, drag effects of the cooling air, and gravity. The following equations are in terms of dimensionless variables (the dimensional and dimensionless variables are defined in Tables 1 and 2). The axial position Z is bounded by $Z = 0$ at the die and $Z = L$ at the upper boundary of the axial domain, which lies just below the guide rolls (see Figure 1). The freeze zone begins at the onset of crystallization and ends at the frost line,

Table 2. Symbols for Dimensionless Variables and Constants

B_1	inflation pressure = $R_0^2\Delta P/(2\mu_0 H_0 V_0)$
B_2	convective heat transfer coefficient = $U_{h0}R_0/(\rho C_{pf} H_0 V_0)$
B_3	heat of crystallization = $\Delta H_{crys} X_f/(C_{pf} T_0)$
B_4	crystallization rate coefficient = $R_0 k_{crys}/V_0$
B_5	dimensionless heat radiation factor = $\sigma_B \varepsilon R_0 T_0^3/(\rho C_{pf} V_0 H_0)$
F_m	elongational or machine tension
F	modified elongational or machine tension
h	film thickness = H/H_0
h_L	film thickness at top boundary of freeze zone = H_L/H_0
$1/h_L$	thickness reduction
r	film bubble-tube radius = R/R_0
r_L	blowup ratio = dimensionless film bubble-tube radius at top boundary of freeze zone = R_L/R_0
χ	crystallinity = X/X_f
υ	film velocity = V/V_0
υ_L	takeup ratio = dimensionless velocity at top boundary of freeze zone = V_L/V_0
β_7	coefficient for temperature dependence of viscosity, β_1/T_0
ς	axial position = Z/R_0
η	viscosity factor = μ/μ_0
θ	temperature = T/T_0
θ_{air}	air temperature = T_{air}/T_0
θ_{max}	temperature at maximum crystallization rate = T_{max}/T_0
$\Delta\theta_{max}$	$\Delta T_{max}/T_0$
θ_w	wall temperature = T_w/T_0
τ	time = tV_0/R_0

where further changes in bubble-tube dimensions are imperceptible due to the extremely large viscosity. In simulations, L is taken to be sufficiently large that the bubble tube is in this frozen state before it reaches $Z = L$.

In the Pearson−Petrie thin-shell model, the dynamic continuity equation takes the form:[25]

$$\psi\left(h\frac{\partial r}{\partial \tau} + r\frac{\partial h}{\partial \tau}\right) + \frac{rhy}{\psi}\frac{\partial y}{\partial \tau} + rh\frac{\partial \upsilon}{\partial \varsigma} + r\upsilon\frac{\partial h}{\partial \varsigma} + h\upsilon y = 0 \tag{1}$$

where $\psi = [1 + (\partial r/\partial\varsigma)^2]^{1/2}$. The dynamic momentum equation in the axial direction is

$$-\frac{r}{\psi}\frac{\partial h}{\partial \tau} + \frac{rhy}{\psi^3}\frac{\partial y}{\partial \tau} + \frac{rh}{\psi^2}\frac{\partial \upsilon}{\partial \varsigma} - \frac{r\upsilon}{\psi^2}\frac{\partial h}{\partial \varsigma} = \frac{F_m + B_1(r^2 - r_f^2)}{2\eta} \tag{2}$$

where

$$y = \frac{\partial r}{\partial \varsigma} \tag{3}$$

F_m is the dimensionless machine tension, B_1 is the dimensionless inflation pressure, and r_f is the value of r at $\varsigma = L/R_0$, and time τ. For the purpose of computing steady-state results and subsequent interpretation, the modified tension $F = F_m - B_1 r_L^2$ is used, which is especially useful as a continuation parameter in getting around turning points when generating blowup ratio versus thickness reduction plots.[3] In this work, however, F is treated as dependent variable, as will be discussed later.

The dynamic momentum equation in the circumferential direction is

$$\psi\frac{h}{r^2}\frac{\partial r}{\partial \tau} + \left(\frac{1}{\psi}\frac{\partial y}{\partial \varsigma} - \frac{\psi}{r}\right)\frac{\partial h}{\partial \tau} - \frac{hy}{\psi^3}\frac{\partial y}{\partial \varsigma}\frac{\partial y}{\partial \tau} - \frac{1}{\psi^2}\frac{\partial y}{\partial \varsigma}\left(h\frac{\partial \upsilon}{\partial \varsigma} - \upsilon\frac{\partial h}{\partial \varsigma}\right) + \frac{\upsilon}{r^2}\left(hy - r\frac{\partial h}{\partial \varsigma}\right) = \frac{B_1}{\eta}\psi^2 \tag{4}$$

The boundary conditions for the Pearson−Petrie model have been the subject of some discussion. At the die, the three boundary conditions for bubble-tube radius, film thickness, and film velocity are

$$r = 1 \text{ at } \varsigma = 0 \tag{5}$$

$$h = 1 \text{ at } \varsigma = 0 \tag{6}$$

$$v = 1 \text{ at } \varsigma = 0 \tag{7}$$

respectively. For the axial gradient of the bubble-tube radius, the "minimally reduced" outflow boundary condition:[26]

$$\psi\frac{h}{r^2}\frac{\partial r}{\partial \tau} + \left(-\frac{\psi}{r}\right)\frac{\partial h}{\partial \tau} + \frac{v}{r^2}\left(hy - r\frac{\partial h}{\partial \varsigma}\right) = \frac{B_1}{\eta}\psi^2 \quad \text{at} \quad \varsigma = L/R_0 \tag{8}$$

was used as previous computations indicated that yields the most physically meaningful results for blown film extrusion,[3] which is consistent with observations in other applications.[26]

Diagonal Form of Continuity and Momentum Equations. Equations 1−4 can be rearranged algebraically into the diagonal form

$$\psi h\frac{\partial r}{\partial \tau} = -\frac{1}{6}\psi^2\left(\frac{F}{\eta} + \frac{B_1 r^2}{\eta}\right) + \frac{2}{3}\psi^2\left(\frac{B_1 r^2}{\eta}\right) + \frac{r}{3}\frac{\partial y}{\partial \varsigma}\left(\frac{F}{\eta} + \frac{B_1 r^2}{\eta}\right) - hvy \tag{9}$$

$$r\psi\frac{\partial h}{\partial \tau} = -rv\frac{\partial h}{\partial \varsigma} - \frac{1}{6}\psi^2\left(\frac{F}{\eta} + \frac{B_1 r^2}{\eta}\right) - \psi^2\frac{B_1 r^2}{3\eta} - \frac{r}{6}\frac{\partial y}{\partial \varsigma}\left(\frac{F}{\eta} + \frac{B_1 r^2}{\eta}\right) \tag{10}$$

$$rhy\frac{\partial y}{\partial \tau} = -\frac{\psi}{3}r\frac{\partial y}{\partial \varsigma}\left(\frac{F}{\eta} + \frac{B_1 r^2}{\eta}\right) + \psi^3\frac{F}{3\eta} - \psi rh\frac{\partial v}{\partial \varsigma} \tag{11}$$

The corresponding "minimally reduced" outflow boundary conditions are

$$\psi h\frac{\partial r}{\partial \tau} = -\frac{1}{6}\psi^2\left(\frac{F}{\eta} + \frac{B_1 r^2}{\eta}\right) + \frac{2}{3}\psi^2\left(\frac{B_1 r^2}{\eta}\right) - hvy \quad \text{at} \quad \varsigma = L/R_0 \tag{12}$$

$$r\psi\frac{\partial h}{\partial \tau} = -rv\frac{\partial h}{\partial \varsigma} - \frac{1}{6}\psi^2\left(\frac{F}{\eta} + \frac{B_1 r^2}{\eta}\right) - \psi^2\frac{B_1 r^2}{3\eta} \quad \text{at} \quad \varsigma = L/R_0 \tag{13}$$

$$rhy\frac{\partial y}{\partial \tau} = \frac{\psi^3}{3}\frac{F}{\eta} - \psi rh\frac{\partial v}{\partial \varsigma} \quad \text{at} \quad \varsigma = L/R_0 \tag{14}$$

Equations 9−14 are useful for stability analysis, as will be discussed later.

The energy balance and crystallization equations are

$$\psi\frac{\partial \theta}{\partial \tau} + v\frac{\partial \theta}{\partial \varsigma} + \psi B_2\frac{\theta - \theta_{air}}{h} + \psi B_5\frac{\theta^4 - \theta_{wall}{}^4}{h} - B_3 B_4 F_\theta(1 - x) = 0 \tag{15}$$

$$\frac{\partial x}{\partial \tau} + v\frac{\partial x}{\partial \varsigma} - B_4 F_\theta(1 - x) = 0 \tag{16}$$

where

$$B_2 = \frac{U_h R_0}{\rho C_{pf} H_0 V_0} \tag{17}$$

$$B_3 = \frac{\Delta H_{crys} X_f}{C_{pf} T_0} \tag{18}$$

$$B_4 = \frac{R_0 k_{crys}}{V_0} \tag{19}$$

$$B_5 = \frac{\varepsilon_{rad}\sigma_B \theta_0{}^3 R_0}{\rho C_{pf} H_0 V_0} \tag{20}$$

The convective heat-loss term takes the form of Newton's law of convective cooling, and the heat loss due to radiation is about 5−20% of that due to convection. The dimensionless air and wall temperatures are defined as

$$\theta_{air} = \frac{T_{air}}{T_0} \tag{21}$$

$$\theta_{wall} = \frac{T_{wall}}{T_0} \tag{22}$$

The function F_θ is the temperature-dependent factor for the rate of crystallization

$$F_\theta = \exp\left[-\frac{4(\ln 2)(\theta - \theta_{max})^2}{(\Delta\theta_{max})^2}\right] \tag{23}$$

where the dimensionless constants θ_{max} and $\Delta\theta_{max}$ are

$$\theta_{max} = \frac{T_{max}}{T_0} \tag{24a}$$

$$\Delta\theta_{max} = \frac{D_{crys}}{T_0} \tag{24b}$$

Unlike the Hoffman−Lauritzen kinetic expression,[27] which has five parameters, this crystallization rate expression has three parameters and allows a finite crystallization rate at the die rather than restricting crystallization to temperatures below the melting point. Like past studies of blown-film extrusion, with the exception of the McHugh group,[11−13] flow-induced crystallization is not included in the model. In this application, other calculations (not shown here) indicated that including flow-induced crystallization in the model resulted in <4% change in computed variables such as inflation pressure, frost line height, and machine tension.

The temperature and degree of crystallization are specified at the die:

$$\theta = 1 \quad \text{at} \quad \varsigma = 0 \tag{25}$$

$$x = 0 \quad \text{at} \quad \varsigma = 0 \tag{26}$$

It is assumed that the bubble air mass M_{air} is constant after the bubble tube is inflated and the inlet air valve is shut due to the sealing of the bubble by the nip rolls. The takeup speed V_L is set by the speed of the nip rolls. The two equations used to set M_{air} and V_L are:

$$M_{air} = \frac{P_{atm} + \Delta P}{R_G T_{air}} R_0{}^3\pi \int_0^{L/R_0} r^2\, d\varsigma \tag{27}$$

$$v = V_L/V_0 \quad \text{at} \quad \varsigma = L/R_0 \tag{28}$$

The two parameters in the momentum equations, B_1 and F, are not set in advance, but are treated as dependent variables (as in ref 3).

Constitutive Relation. A nonisothermal quasi-Newtonian constitutive relation was used for LLDPE that accounts for the effect of temperature and crystallization on the viscosity of the extruded polymer. The viscosity was described by

$$\mu = \mu_0 \eta \tag{29}$$

where the base viscosity μ_0 is

$$\mu_0 = \alpha_1 \exp\left(\frac{\beta_1}{T_0}\right) \tag{30}$$

and the dimensionless viscosity factor η is

$$\eta = \exp\left[\frac{\beta_1}{T_0}\left(\frac{1}{\theta} - 1\right)\right]\exp(\alpha_2 \chi^{\beta_2}) \tag{31}$$

where α_1, α_2, β_1, and β_2 are measured or adjusted constants. This model does not take deformation thinning of LLDPE into account as this would be relatively small for this particular type of polymer.[9]

Heat Transfer Expression. The heat transfer coefficient U_h from the film to the external air is a function of the position Z above the die. The air from the experimental air ring impinges on the bubble surface at $\varsigma \sim A_H$. Turbulent flow simulations indicate that the heat transfer coefficient for a single-lip air ring reaches a maximum before dropping to a lower value.[24] These results suggest that the heat transfer coefficient can be assumed to have the spatial form

$$U_h = \begin{cases} 0 & \text{for } \varsigma \le A_H \\ U_{h,0} \exp\left(-\dfrac{\varsigma - A_H}{B_H}\right) & \text{for } A_H < \varsigma \le C_H \\ 0 & \text{for } \varsigma > C_H \end{cases} \tag{32}$$

since U_h is expected to (1) be negligible near the die as the air ring blocks access to the bubble surface, (2) abruptly reach a maximum as the cooling air impinges upon the bubble surface, and (3) decline to a lower value before becoming negligible.

Numerical Methods

Model Simulation. The system of algebraic and partial differential equations was solved using the numerical method of lines (NMOL),[28] which discretizes the equations in the spatial variable ς at a number of grid points N_Z. Spatial derivatives such as $\partial v/\partial \varsigma$ were approximated by five-point finite differences that were fourth-order accurate using the variable-grid spacing implementation in the subroutine DSS032.[29] The second-derivative $\partial^2 r/\partial \varsigma^2$ was approximated with five-point central differences using a formula by Fornberg.[30] The spatial discretization converted (1), (2), (4), (8), (15), and (16) to a set of $(5N_Z + 1)$ coupled ordinary differential equations containing time derivatives for the values of r, h, y, θ, and x at each grid point. Upon discretization, (3) results in a set of N_Z algebraic equations (no time derivatives), and the boundary conditions (5)−(7), (25), and (26) are algebraic equations. The resulting system of ordinary differential and algebraic equations (DAEs) was solved using the solver DASPK3.0.[31,32] All computations were performed in double-precision Fortran 77 using a 2.66 GHz Intel duo-core processor-based computer.

Table 3. Values of the Constants Used in All of the Simulations[a]

b	0.68
C_{pf}	2.427 kJ/kg·K
H_0	0.05 cm
k_{crys}	0.37 1/s
L	0.4068 m
R_0	1.25 cm
T_{air}	319 K
T_{max}	368 K
ΔT_{max}	5 K
T_0	481.2 K
V_0	0.46803 cm/s
α_1	0.688 Pa·s
α_2	20.0
β_1	4388 K
β_2	1.0
X_f	0.50
ΔH_{crys}	294.1 kJ/kg
ρ	920 kg/m^3
τ_s	100.0

[a] The key physical properties of the polymer and the kinetic rate constants of crystallization are the same as those reported by Henrichsen and McHugh[13] except for ΔT_{max} and α_2 which were reduced by a factor of 10 (α_2 is referred to as F_{sc} in the work of Henrichsen and McHugh[13]).

The calculations started with a low number of grid points, about 101, and these were increased until the computed results were unchanged within a minimum of four significant figures of accuracy. The grid point allocation that met this criterion for all of the cases considered was 141 points uniformly distributed from $\varsigma = 0$ to 0.4 L/R_0, and 60 points uniformly distributed from $\varsigma = 0.4$ to 1.0 L/R_0. Spatial derivatives were approximated by using five-point biased upwind differences for $\partial r/\partial \varsigma$, $\partial h/\partial \varsigma$, $\partial v/\partial \varsigma$, $\partial \theta/\partial \varsigma$, and $\partial x/\partial \varsigma$ and using five-point centered differences for $\partial^2 r/\partial \varsigma^2$.

The startup condition used in the calculations consisted of extruding and attaching the bubble tube to the nip rolls under conditions of uniform (with respect to Z) bubble-tube radius and film thickness. The set values for the bubble air mass M_{air} and takeup speed V_L were then increased from zero to positive values by using the switching functions:

$$(M_{air} - M_{air,0})(1 - \exp(-\tau^2/\tau_s^2)) + M_{air,0} \tag{33}$$

$$(V_L - V_{L,0})(1 - \exp(-\tau^2/\tau_s^2)) + V_{L,0} \tag{34}$$

where τ_s is a switching time constant and $M_{air,0}$ and $V_{L,0}$ are the initial values of bubble air mass and takeup speed, respectively. The value of M_{air} was determined from the experimental bubble geometry and V_L was set by the speed of the nip rolls.

Parameter Estimation. The values of the equipment dimensions, polymer properties, and unchanged operating conditions used in the computer simulations are reported in Table 3. Table 4 lists the set conditions and measured data for each experiment. The objective was to fit the convective heat transfer coefficient to experimental bubble radius and temperature profiles. The values of the four parameters $U_{h,0}$, A_H, B_H, and C_H in the heat transfer coefficient (32) were adjusted to minimize the weighted sum-of-squared-errors between the simulated and experimental outputs:[33]

$$S = \sum_{i=1}^{M_r}\left[\frac{(r_i - r_{exp,i})^2}{\sigma_r^2}\right] + \sum_{i=1}^{M_\theta}\left[\frac{(\theta_i - \theta_{exp,i})^2}{\sigma_\theta^2}\right] \tag{35}$$

where the index i refers to the axial position where a measurement was made, M_r is the total number of bubble radius measurements, M_θ is the total number of temperature measure-

Table 4. Experimental Data from a Laboratory Blown Film Extruder

experiment number	cooling air flow rate, m/s	T_0, K	measured ΔP, Pa	measured blowup ratio	set takeup ratio	measured thickness reduction	measured M_{air}, kg·mol
10	1.5	481.2	107	2.306	4.646	10.71	0.03707
11	1.5	481.6	109	2.225	5.342	11.81	0.03413
12	1.5	481.1	112	2.144	5.989	12.80	0.03159
13	1.5	481.8	112	2.073	6.644	13.75	0.02921
14	1.5	482.0	113	2.012	7.299	14.68	0.02732
15	1.5	482.8	113	1.941	7.963	15.45	0.02525
25	1.0	482.0	104	2.225	3.988	8.79	0.03522
26	1.0	482.0	107	2.144	5.306	11.17	0.03207
27	1.0	483.0	109	2.073	6.624	13.50	0.03024
28	1.0	483.0	113	2.012	7.977	15.69	0.02796
29	1.0	482.0	115	1.859	9.294	17.28	0.02358
30	1.0	483.0	116	1.859	10.612	19.26	0.02261

Table 5. Best-Fit Model Parameters for the Heat Transfer Coefficient

experiment number	cooling air w rate, m/s	A_H	B_H	C_H
10−15	1.5	2.5	5.00	32.544(= L/R_0)
25−26	1.0	2.0	9.28	10.00
27−30	1.0	2.0	9.28	13.00

ments, r_i and θ_i are the model predictions at the axial position i for the dimensionless bubble radius and temperature, respectively, the subscript "exp" refers to the experimental value, and the variance of the measurements for the dimensionless bubble radius and temperature are σ_r^2 and σ_θ^2, respectively. This selection for the weights in (35) results in the maximum-likelihood estimates for the model parameters.[33]

For experiments 10 and 25, the minimization with respect to $U_{h,0}$, A_H, B_H, and C_H was implemented using DBCLSF, which is the IMSL Marquardt−Levenberg optimization algorithm available in the Professional Edition of the Microsoft Fortran Power Station software package. This code allows the placement of upper and lower bounds on the optimization parameters to avoid parameter values where physically realistic solutions for the blown film extrusion model do not exist. Experiments 10−15 and 25−30 represent operations where the cooling air flow is high and low, respectively. On the basis of the equipment design and the convective heat transfer mechanism,[24] the values of A_H, B_H, and C_H are expected to be essentially the same for experiments with the same cooling air flow rate and so should have the same value within experiments 10−15 and the same value within experiments 25−30. As such, the values of A_H, B_H, and C_H obtained by parameter estimation from experiment 10 data were retained for experiments 11−15, so that only $U_{h,0}$ was used in the Levenberg−Marquardt minimization. The same approach was repeated for experiments 26−30 based on the A_H and B_H obtained from experiment 25 data, whereas C_H was increased for experiments 27−30 to improve the fit. The values of A_H, B_H, and C_H are reported in Table 5.

Blown Film Extruder Experimental Methods

Figure 2 is a photograph of a laboratory-scale blown film extruder located at the University of Illinois. Linear low density polyethylene (LLDPE, Dowlex 2045, density = 0.920 g/cm^3) was supplied by Dow Chemical Company. LLDPE was extruded through a Haake Rheomex 254 single-screw extruder (19.1 mm diameter, 25:1 L/D ratio) connected to a Rheodrive 5000 and equipped with a blown film die (25 mm diameter, 24 mm inner ring diameter). The extruder barrel zone temperatures were set to 180, 190, and 200 °C for all experiments. The die temperature was set to 200 °C, which resulted in melt temperature of 207−210 °C. The inflation air, cooling air, and takeup speed were set via a Haake FP2 Film Postex blown film takeoff unit. The inflation pressure of the bubble was measured using an Omega PX139 pressure transducer. The flow rate and temperature of the cooling air were measured using an Airflow TA35 thermal anemometer. The thermal anemometer was also used to measure the room temperature.

Online measurements from the blown film extruder such as the extruder barrel temperatures, melt temperature, melt pressure, inflation pressure, and takeup speed were acquired using a Data Translation DT3004 data acquisition board. The bubble temperature was measured using a Raytek P3 infrared thermometer (wavelength = 3.43 μm) connected to Raytek Thermalert 3Plus. The axial position of the infrared thermometer was controlled using a Velmex BiSlide linear motion system connected to Panther LI2 microstepper (Intelligent Motion Systems, Inc.). Images of the blown film bubble were captured using a Pulnix TMC-6700 progressive scan CCD digital camera and XCAP image processing software by Epix. The bubble diameter profile was obtained from image analysis of the captured images. The film width and thickness were measured offline using a ruler and a caliper. To measure the mass flow rate, the melt near the die exit was marked every minute and film strips weighed.

Twelve sets of experimental data collected from the laboratory extruder were used for parameter estimation (see Table 4 for the measured bubble inflation pressures, die conditions, and the measured blowup and takeup ratios). Experiments 10−15 were performed on July 2, 2004, and experiments 25−30 were performed on July 9, 2004. On each day, most of the conditions such as extrusion rate, extrusion temperature, and cooling air flow rate were held constant within the experimental tolerances of the extruder and the takeup ratio was varied. Upon a change

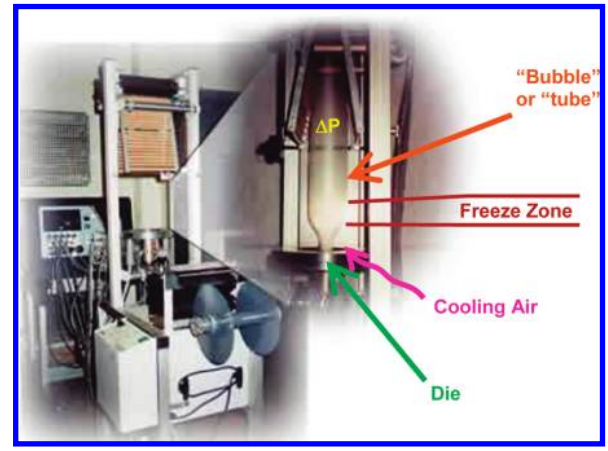

Figure 2. Experimental blown film extruder (left) with zoomed-in photograph (upper right).

Table 6. Simulation Results for Thin-Shell Model with Best-Fit Heat Transfer Coefficient $U_{h,0}$

	values of fitted parameters			model simulation results		
exp no.	$U_{h,0}$, W/K·m^2	calculated ΔP, Pa	calculated F	thickness reduction	blowup ratio	eigenvalues with maximum real part
10	67.03	81.6	1.278	10.75	2.313	$-0.029 \pm 0.99i$
11	67.03	98.33	1.609	11.84	2.217	$-0.035 \pm 1.13i$
12	67.03	104.1	1.690	12.79	2.136	$-0.030 \pm 1.28i$
13	67.03	107.2	1.759	13.66	2.056	$-0.023 \pm 1.43i$
14	67.03	113.4	1.819	14.53	1.990	$-0.016 \pm 1.58i$
15	67.03	113.8	1.868	15.24	1.915	$-0.006 \pm 1.73i$
25	60.74	94.2	1.469	8.914	2.235	$-0.015 \pm 0.83i$
26	54.46	103.7	1.662	11.41	2.150	$-0.015 \pm 1.12i$
27	51.32	108.7	1.797	13.93	2.103	$-0.0001 \pm 1.42i$
28	62.84	120.9	2.036	16.14	2.023	$-0.006 \pm 1.71i$
29	68.00	131.9	2.208	17.43	1.861	$0.011 \pm 2.00i$
30	75.04	oscillations	oscillations	oscillations	oscillations	not applicable

in takeup ratio, all measurements were collected after the air bubble reached a new steady state, which took about 10 min. The bubble air mass declined from experiment to experiment on each of the two days, which indicates that some air leaked from the bubble. The bubble air mass was fairly constant over the measurement period (about a minute or so) in which each data set was collected.

Results and Discussion

The best-fit heat transfer coefficient $U_{h,0}$ and associated simulation outputs are reported in Table 5. The experimentally observed values of the takeup ratio and bubble air mass were set in the calculations. The inflation pressure ΔP and F were generated by the solution of the model. Two operational variables, thickness reduction and blowup ratio, are well fit by the model, within experimental error (compare Tables 4 and 5). The measured value of M_{air} declines as takeup ratio is increased, which may indicate a slow air leak during the establishment of new steady states.

The calculated inflation pressures in Table 6 approximate the measured values, which are accurate only to 10−20%, shown in Table 4. The slight differences can be explained by Venturi and Coanda effects and lowering of the outside surface pressure.[34−37] In particular, some studies indicate that the external air flow over the outer bubble surface reduces surface pressures and thereby increases effective inflation pressure.[34,38]

A single value for the heat transfer coefficient $U_{h,0}$ (67.03 W/m^2·K; see Table 6) was able to fit the thickness reduction and blowup ratio for an airflow velocity of 1.5 m/s, and this value of the best-fit heat transfer coefficient $U_{h,0}$ is within the range of fitted values for the cooling air flow rate of 1.0 m/s (51.32−75.04 W/m^2·K) for experiments 25−30. The experimentally determined spatial profiles for the radii and temperature were very well fit for all experiments except for experiment 30 for which the simulations yielded large oscillations. A simple boundary-layer model would indicate that a higher cooling air

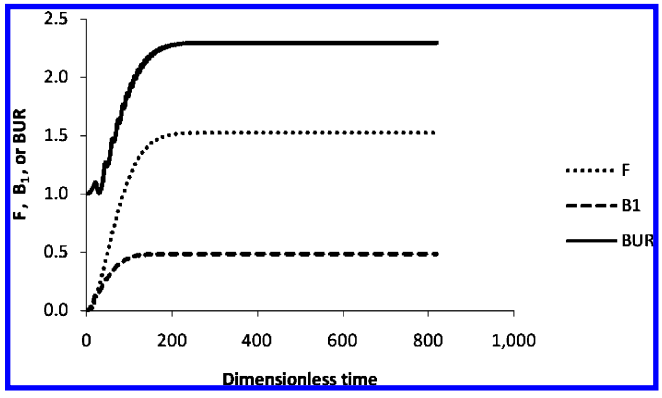

Figure 3. Evolution of the modified machine tension F, inflation pressure B_1, and blowup ratio (BUR) under stable conditions for experiment 10.

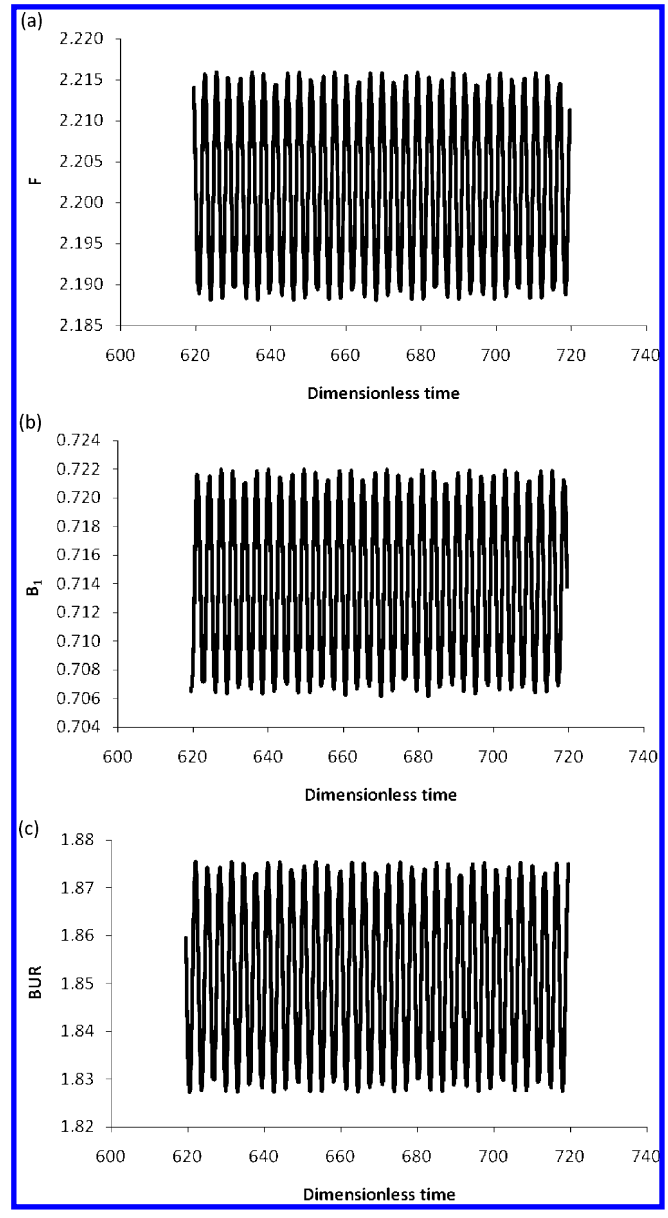

Figure 4. Asymptotic oscillations of the (a) modified machine tension F, (b) inflation pressure B_1, and (c) blowup ratio (BUR) for the conditions of experiment 29.

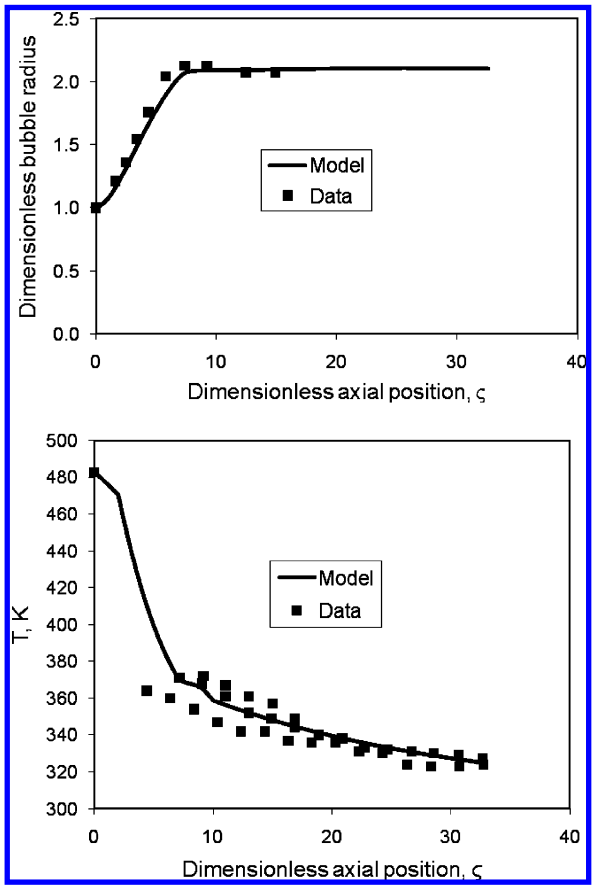

Figure 5. Comparison of the thin-shell model with measured profiles for the (top) bubble radius and (bottom) temperature for experiment 29.

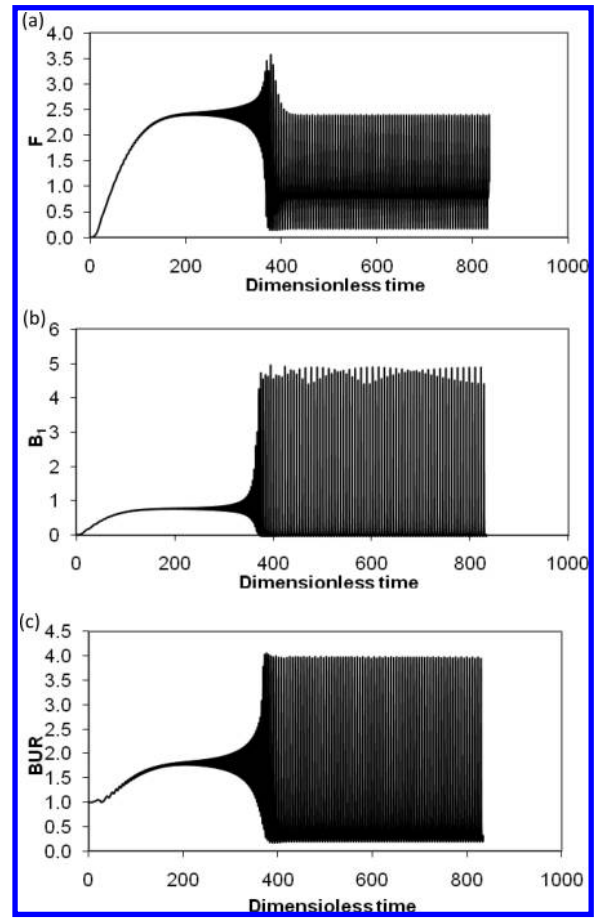

Figure 6. Dynamic simulation of the (a) modified machine tension F, (b) inflation pressure B_1, and (c) blowup ratio (BUR) for the conditions of experiment 30.

flow rate should result in higher values of the heat transfer coefficient $U_{h,0}$, which is seen for most but not all of the experimental conditions in Table 6. This provides some support for the notion that fairly complicated heat transfer effects occur as a function of airflow velocity and bubble size, which has been discussed by others.[34−38]

Figure 3 shows the evolution of the modified machine tension F, inflation pressure B_1, and blowup ratio as the bubble air mass M_{air} and takeup speed are switched to their set values for experiment 10. Using a switching time of 100 dimensionless time units (time in seconds divided by R_0/V_0), the steady-state values were reached in <400 dimensionless time units. The slight blip in the blowup ratio versus time curve in Figure 3 disappears for a switching time of 400 dimensionless time units but does not create any numerical issues since only the steady-state values were compared to data. The use of switching functions allowed a steady-state to be reached for the thin-shell model in a computationally stable manner within 1000 s of simulated time.

Table 6 reports the eigenvalues of the linearization of the DAE system with the maximum real component for each of the experimental conditions (for background on the stability analysis of DAE systems, see the work of Stykel,[39] for example). The dynamic simulation model was locally asymptotically stable for ten of the experimental conditions (10−15, 25−28), and not locally asymptotically stable for two experimental conditions (29 and 30). The dynamic responses for experiment 29, which had two eigenvalues with positive real parts, had oscillations of very small magnitude about steady-state operations (see Figure 4) with only a small effect on the spatial profiles (see Figure 5). This transition from a stable steady-state to a very small magnitude oscillation about an unstable steady-state is a Hopf bifurcation[40] (for stability analyses of other blown

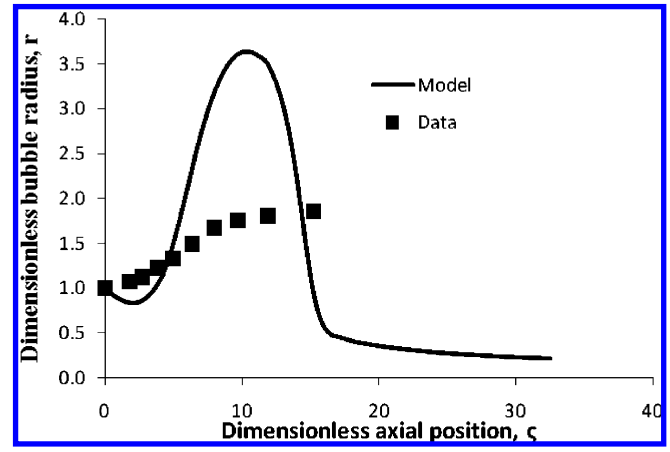

Figure 7. Snapshot of the simulated and experimental bubble radius profile for experiment 30 ($\tau = 820$).

extrusion models see refs 15, 25, and 41−43). Dynamic simulations indicate convergence to a chaotic oscillation for the conditions of experiment 30 (see Figure 6). A representative snapshot of the computed bubble radius profile for experiment 30 is shown in Figure 7, showing a very poor fit to the data. The experimental extruder had a wider range of stable asymptotic operations than the simulation model.

Representative bubble radius and film temperature profiles obtained from experiments and from the simulation model with the best-fit heat transfer coefficient are shown in Figures 5 and 8−10. Among the first set of experiments with a cooling air flow rate of 1.5 m/s, experiment 10 had the lowest takeup ratio,

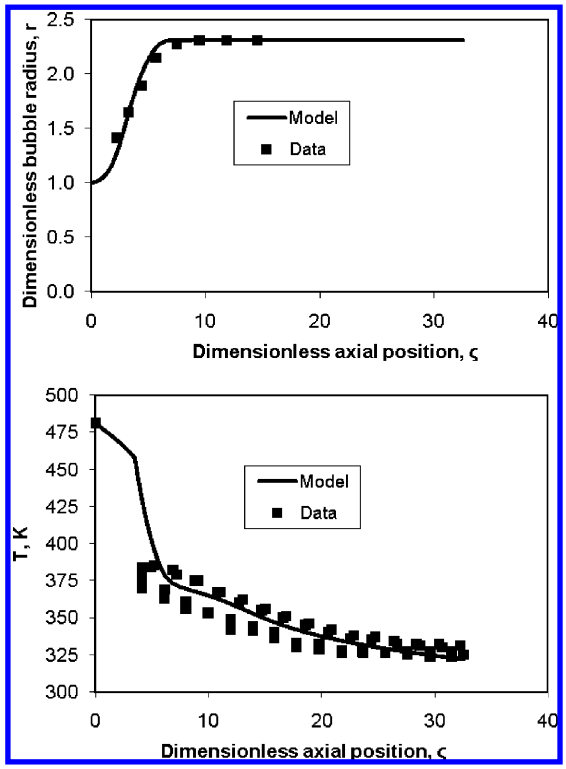

Figure 8. Comparison of the thin-shell model with measured profiles for the (top) bubble radius and (bottom) temperature for experiment 10.

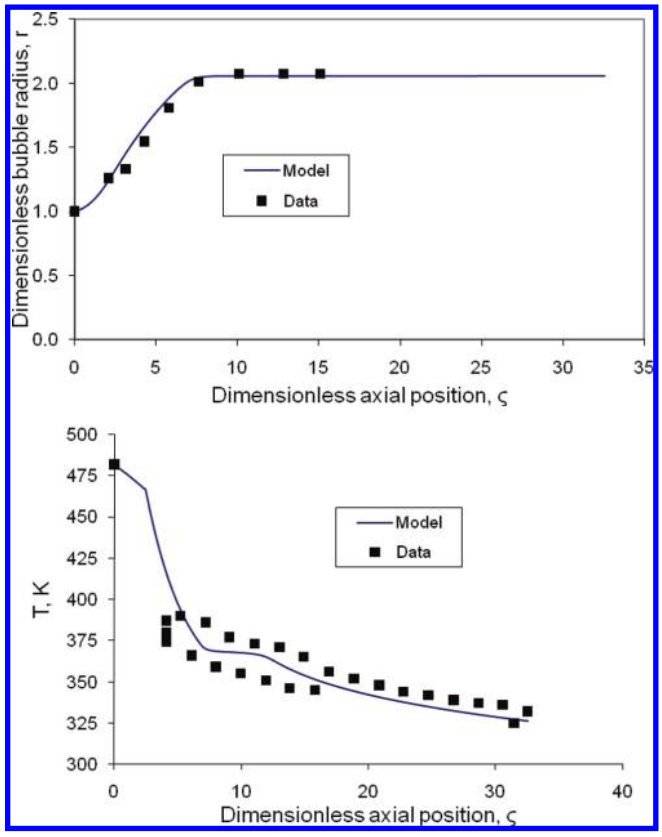

Figure 9. Comparison of the thin-shell model with measured profiles for the (top) bubble radius and (bottom) temperature for experiment 13.

which resulted in a longer residence time for the polymer film, the larger final bubble radius, and a thicker final film (Table 4). The bubble radius approached its final value at a lower axial position for experiment 10 than for other experiments (for example, compare Figures 8 and 9). The same trends are

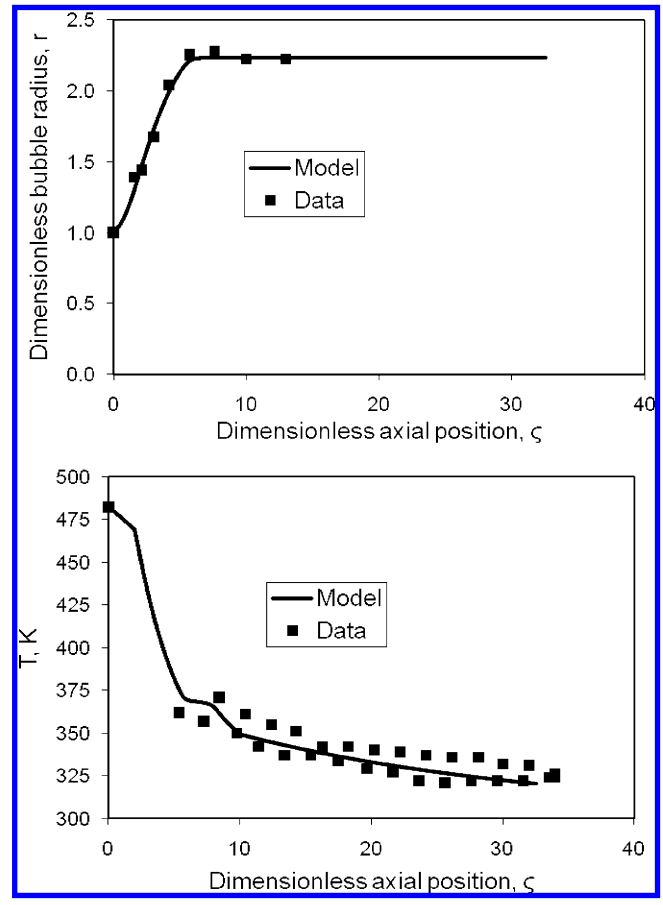

Figure 10. Comparison of the thin-shell model with measured profiles for the (top) bubble radius and (bottom) temperature for experiment 25.

observed for the second set of experiments with a cooling air flow rate of 1.0 m/s (see Table 4 and compare Figures 5 and 10). The spatial profiles obtained from the simulation models agree within the statistical scatter of the experimental data.

Conclusions

Using a small number of fitting parameters, the thin-shell quasi-Newtonian model was fit to experimental data when the bubble air mass was calculated from the measured profile of the bubble radius and the takeup speed was set by the speed of the nip rolls. Using the known values of M_{air} and takeup speed, the model generated spatial profiles of the bubble geometry and film temperature that were identical to those observed in experiments (e.g., see Figures 5 and 8−10). Adjustment of the constants in a heat transfer coefficient expression (32) that was qualitatively consistent with turbulent fluid mechanics calculations for the air flows inside and outside of the tubular film was enough to bring the model bubble radius and temperature profiles into agreement with experiments.

The calculated inflation pressures were, for the most part, within the experimental uncertainty of the measured inflation pressures (compare Tables 4 and 6). The moderate differences can be explained by previous studies indicating that the external air flow over the outer bubble surface changes surface pressures and thereby alters effective inflation pressure.[34,38] A single heat transfer expression fit the experimental conditions for a cooling air flow rate of 1.5 m/s, whereas the variation of a single parameter was able to fit all but one experimental condition for a cooling air flow rate of 1.0 m/s. The experimental condition that was poorly fit by the model had the highest takeup ratio,

which was the operating condition closest to film instability and likely the condition most sensitive to the heat transfer relation. The experimental conditions corresponding to observed stable operations were quite consistent with linearized stability analysis applied to the model with best-fit parameters (see Table 6).

Acknowledgment

The Procter and Gamble Company is acknowledged for partial research support, and Dow Chemical Company is acknowledged for providing polymer beads.

Literature Cited

(1) Middleman, S. *Fundamental Studies of Polymer Processing*; McGraw-Hill: New York, 1977.

(2) Cantor, K. *Blown Film Extrusion: An Introduction*; Hanser: Munich, 2006.

(3) Pirkle, J. C., Jr.; Braatz, R. D. Dynamic Modeling of Blown Film Extrusion. *Polym. Eng. Sci.* **2003**, *43*, 398.

(4) Pirkle, J. C., Jr.; Braatz, R. D. Comparison of the Dynamic Thin Shell and Quasi-cylindrical Models for Blown Film Extrusion. *Polym. Eng. Sci.* **2004**, *44*, 1267.

(5) Pearson, J. R. A.; Petrie, C. J. S. The Flow of a Tubular Film. Part 1. Formal Mathematical Representation. *J. Fluid Mech.* **1970**, *40*, 1.

(6) Pearson, J. R. A.; Petrie, C. J. S. The Flow of a Tubular Film. Part 2. Interpretation of the Model and Discussion of the Solutions. *J. Fluid Mech.* **1970**, *42*, 609.

(7) Pearson, J. R. A.; Petrie, C. J. S. A Fluid-mechanical Analysis of the Film-blowing Process. *Plast. Polym.* **1970**, *38*, 85.

(8) Liu, C.-C. Studies of Mathematical Modeling and Experimental On-Line Measurement Techniques for the Tubular Film Blowing Process. M.S. Thesis. Dept. of Materials Science and Engineering. University of Tennessee: Knoxville, 1991.

(9) Liu, C.-C. On-Line Experimental Study and Theoretical Modeling of Tubular Film Blowing. Ph.D. Thesis. Dept. of Materials Science and Engineering, University of Tennessee: Knoxville, 1994.

(10) Liu, C.-C.; Bogue, D. C.; Spruiell, J. E. Tubular Film Blowing. Part 2. Theoretical Modeling. *Int. Polym. Process.* **1995**, *10*, 230.

(11) Doufas, A. K.; McHugh, A. J. Simulation of Film Blowing Including Flow-induced Crystallization. Model Development and Predictions. *J. Rheol.* **2001**, *45*, 1085.

(12) Henrichsen, L. K.; McHugh, A. J.; Cherukupalli, S. S.; Ogale, A. A. Microstructure and Kinematic Aspects of Blown Film Extrusion Process: II. Numerical Modeling and Prediction of LLDPE and LDPE. *Plast. Rubbers Compos.* **2004**, *33*, 383.

(13) Henrichsen, L. K.; McHugh, A. J. Analysis of Film Blowing with Flow-enhanced Crystallization. Part. I. Steady-state Behavior. *Int. Polym. Process.* **2007**, *22*, 179.

(14) Khonakdar, H. A.; Morshedian, J.; Nodehi, A. O. Mathematical and Computational Modeling of Heat Transfer and Deformation in Film Blowing Process. *J. Appl. Polym. Sci.* **2002**, *86*, 2115.

(15) Hyun, J. C.; Kim, H.; Lee, J. S.; Song, H.-S.; Jung, H. W. Transient Solutions of the Dynamics in Film Blowing Processes. *J. Non-Newtonian Fluid Mech.* **2004**, *121*, 157.

(16) Pirkle, Jr., J. C.; Braatz, R. D. A Thin-shell Two-phase Microstructural Model for Blown Film Extrusion. *J. Rheol.*, **2010**, in press.

(17) Cao, B.; Campbell, G. A. Viscoplastic-elastic Modeling of Tubular Blown Film Processing. *AIChE J.* **1990**, *36*, 420.

(18) Phan-Thien, N.; Tanner, R. I. New Constitutive Equation Derived from Network Theory. *J. Non-Newtonian Fluid Mech.* **1977**, *2*, 353.

(19) Phan-Thien, N. A Nonlinear Network Viscoelastic Model. *J. Rheol.* **1978**, *22*, 259.

(20) Muslet, I. A.; Kamal, M. R. Computer Simulation of the Film Blowing Process Incorporating Crystallization and Viscoelasticity. *J. Rheol.* **2004**, *48*, 525.

(21) Muke, S.; Connell, H.; Sbarski, H.; Bhattacharya, S. N. Numerical Modeling and Experimental Verification of Blown Film Processing. *J. Non-Newtonian Fluid Mech.* **2003**, *116*, 113.

(22) Khan, A.; Shepherd, J. J.; Bhattacharya, S. Numerical Modeling of the Effect of Operating Parameters in the Plastic Blown Film Process. *ANZIAM J.* **2005**, *46*, C1239.

(23) Alaie, S. M.; Papanastasiou, T. C. Modeling of Non-isothermal Film Blowing with Integral Constitutive Equations. *Int. Polym. Process.* **1993**, *8*, 51.

(24) Sidiropoulos, V.; Wood, P. E.; Vlachopoulos, J. The Aerodynamics of Cooling of Blown Film Bubbles. *J. Reinf. Plast. Comp.* **1999**, *18*, 529.

(25) Yoon, K.-S.; Park, C.-W. Stability of a Blown Film Extrusion Process. *Intern. Polym. Process.* **1999**, *XIV*, 342.

(26) Schiesser, W. E. PDE Boundary Conditions from Minimum Reduction of the PDE. *Appl. Numer. Math.* **1996**, *20*, 171.

(27) Hoffman, J. D.; Davis, G. T.; Lauritzen, J. I. The Rate of Crystallization of Linear Polymers. In *Treatise on Solid State Chemistry: Crystallization and Non-crystalline Solids*; Hanney, J. B., Ed.; Plenum: New York, 1976; Chapter 7, Vol. 3.

(28) Schiesser, W. E. *The Numerical Method of Lines Integration of Partial Differential Equations*; Academic Press: San Diego, 1991.

(29) Silebi, C. A.; Schiesser, W. E. *Dynamic Modeling of Transport Process Systems*; Academic Press: San Diego, 1992.

(30) Fornberg, B. Calculation of Weights in Finite Difference Formulas. *SIAM Rev.* **1998**, *40*, 685.

(31) Petzold, L. R. A Description of DASSL: A Differential/algebraic System Solver. In *Scientific Computing*; Stepleman, R. S., Ed.; IMACS: North-Holland, 1983; pp 65−68.

(32) Maly, T.; Petzold, L. R. Numerical Methods and Software for Sensitivity Analysis of Differential-Algebraic Systems. *Appl. Numer. Math.* **1996**, *20*, 41.

(33) Beck, J. V.; Arnold, K. J. *Parameter Estimation in Engineering and Science*; Wiley: New York, 1977.

(34) Akaike, O.; Tsuiji, T.; Nagano, Y. Simulation of Blown-film process Taking Account of Cooling-Air Effect. *Intern. Polym. Process.* **1999**, *14*, 168.

(35) Campbell, G. A. N. T.; Obot, N. T.; Cao, B. Aerodynamics in the Blown Film Process. *Polym. Eng. Sci.* **1992**, *32*, 751.

(36) Sidiropoulos, V.; Vlachopoulos, V. An Investigation of Venturi and Coanda Effects in Blown Film Cooling. *Int. Polym. Process.* **2000**, *15*, 40.

(37) Sidiropoulos, V.; Vlachopoulos, V. Numerical Simulations of Blown Film Cooling. *J. Reinf. Plast. Compos.* **2002**, *21*, 629.

(38) Gao, N. S.; Li, N. S.; D. Ewing, D. Investigation of the Cooling Jets Used in the Blown Film Process. *Int. Polym. Process.* **2005**, *20*, 68.

(39) Stykel, T. On Criteria for Asymptotic Stability of Differential-Algebraic systems. *Angew. Math. Mech.* **2002**, *82*, 147.

(40) Seidel, R. *From Equilibrium to Chaos: Practical Bifurcation and Stability Analysis*; Elsevier: Amsterdam, 1988.

(41) Cain, J. J.; Denn, M. M. Multiplicities and Instabilities in Film Blowing. *Polym. Eng. Sci.* **1988**, *28*, 1527.

(42) Lee, J. S.; Shin, D. M.; Song, H.-S.; Jung, H. W.; Hyun, J. C. Existence of Optimal Cooling Conditions in the Film Blowing Process. *J. Non-Newtonian Fluid Mech.* **2006**, *137*, 24.

(43) Shin, D. M.; Lee, J. S.; Jung, H. W.; Hyun, J. C. Multiplicity, Bifurcation, Stability and Hysteresis in Dynamic Solutions of Film Blowing Process. *J. Rheol.* **2007**, *51*, 605.

Received for review January 26, 2010
Revised manuscript received March 19, 2010
Accepted March 25, 2010

IE100188G